Available online at www.sciencedirect.com

ScienceDirect

Procedia Manufacturing 34 (2019) 65–72

Procedia MANUFACTURING

www.elsevier.com/locate/procedia

47th SME North American Manufacturing Research Conference, Penn State Behrend Erie, Pennsylvania, 2019

# Experimental and numerical analysis of roller burnishing of *Waspaloy*

Sergio Rinaldi[a]*, Giovanna Rotella[b], Domenico Umbrello[a]

[a]*Department of Mechanical, Energy and Management Engineering, University of Calabria, Rende, CS 87036, Italy*
[b]*Department of Computer Engineering, Modeling, Electronics and Systems Engineering, University of Calabria, Rende, CS 87036, Italy*

* Corresponding author. Tel.: +39-0984-494637. *E-mail address:* sergio.rinaldi@unical.it

**Abstract**

Nickel based superalloys, such as *Waspaloy*, are extensively used for applications under heavy environmental conditions due to their superior thermo-mechanical properties. However, manufacturing processes of these materials are challenging since they involve issues related to their poor workability. Thus, huge research work for optimizing the processing parameters is still required. This problem becomes even more pronounced when finishing processes, such as roller burnishing, are considered. In fact, it is crucial to use parameters able to increase the productivity and to improve the quality of the manufactured parts, consequently a huge number of preliminary experimental tests have to be carried out. Hence, numerical simulation can be a valid support for obtaining information about the metallurgical phenomena that affect the materials while large strains occur. However, commercial software are not still able to appropriately predict such modifications. Thus, the main objective of the present work is to study a roller burnishing on *Waspaloy* in terms of processing parameters and surface integrity by experimental and numerical analysis, in terms of forces, temperatures, roughness, microstructural modification and microhardness. Thus, the customized simulation demonstrated to provide useful information able to drastically reduce the number of needed tests leading also to a deeper knowledge of the microscopic phenomena involved in the process.

© 2019 The Authors. Published by Elsevier B.V.
This is an open access article under the CC BY-NC-ND license (http://creativecommons.org/licenses/by-nc-nd/3.0/)
Peer-review under responsibility of the Scientific Committee of NAMRI/SME.

*Keywords:* Roller burnishing; *Waspaloy*; Physics based numerical modeling; Surface Integrity

## 1. Introduction

A large number of components used in aerospace, chemical and nuclear industries, spend their life working under critical conditions such as high temperatures, cyclical loading etc. Therefore, an important role in their design is played by safety and reliability. Mechanical and thermal cycling loads induce many microscopic phenomena, such as slip band formation, which could lead to the product abrupt failure due to crack nucleation and propagation [1].

For these reasons surface improvements are required in order to avoid or at least retard the initiation of critical defects and subsequently their failure. Thus, surface integrity enhancement e.g. surface roughness reduction, surface hardening may lead to the production of high quality components with improved performance [2].

In order to meet the desired surface requirements and accomplish the needs of mass production, many superfinishing processes have been designed such as roller-burnishing process which has been proved to have beneficial effects on surface integrity [3].

In burnishing processes a smooth rigid tool with different possible shapes (roller, ball, diamond, etc.) is compressed on the workpiece surface in order to plastically deform the contact surface and sub-surface in order to enhance its properties [4].

In detail, roller-burnishing process improves the surface roughness displacing the asperities into the valleys of the worked surface. Thus, smoother and uniform surfaces involving an extremely low wear rate are produced after burnishing. Moreover, the burnished surface results harder than the bulk and the process induces a consistent state of compressive residual stresses [5].

2351-9789 © 2019 The Authors. Published by Elsevier B.V.
This is an open access article under the CC BY-NC-ND license (http://creativecommons.org/licenses/by-nc-nd/3.0/)
Peer-review under responsibility of the Scientific Committee of NAMRI/SME.
10.1016/j.promfg.2019.06.118

This promising process, is not yet massively employed in industry due to the lack of knowledge on the optimal process parameters and their influence on the surface characteristics. This problem is more evident when high strength materials such as *Ti* and *Ni-Cr* alloys are employed. These materials demonstrate strong mechanical properties even under heavy thermo-mechanical loads. In particular, *Waspaloy* shows important mechanical properties as stiffness, wear and corrosion resistance. On the other hand, the mechanical characteristics of superalloys affect their workability and the related literature shows still a lack of complete information regarding their workability [6].

The selection of the right configuration of processing parameters is crucial to achieve the desired surface integrity on the manufactured component. Therefore, a high number of tests is required to find a useful process parameters combinations able to manufacture the desired surface. Thus, tools able to predict the material thermo-mechanical behavior and the evolution of the microstructure during the burnishing process are extremely useful [7].

In particular, a physics-based model can be extremely helpful to accurately describe the microstructural phenomena taking place during large deformations generated at varying process parameters [8]. This paper shows the influence of roller-burnishing parameters on surface integrity of *Waspaloy* by experimental and numerical data. In particular, the numerical analysis provides deeper information on the microstructural changes mechanism taking place during the process which can be employed to improve the surface integrity of the burnished products. The obtained results involve process (forces and temperatures) and surface integrity (surface roughness, micro-hardness, etc.) variables, supplying a deeper knowledge on the effects of burnishing parameters on *Waspaloy* surface characteristics.

**Nomenclature**

| | |
|---|---|
| $F_b$ | burnishing force |
| $F_t$ | tangential force |
| $T$ | Temperature at the contact surface |
| $V_b$ | burnishing speed |
| $f$ | feed rate |
| $N$ | number of passes |
| $h_{int}$ | global heat transfer coefficient ($h_{int}$) |
| $\varepsilon^p$ | plastic strain |
| $\dot{\varepsilon}^p$ | plastic strain rate |
| $\sigma_{pl}$ | plastic flow stress |
| $\sigma^*$ | stress due to short range barriers |
| $\sigma_G$ | stress due to dislocation hardening |
| $\sigma_{HP}$ | Hall-Petch stress |
| $\Delta h$ | hardness increment |
| $k_h$ | calibration constant |
| $M$ | Taylor Factor |
| $\alpha$ | material constant |
| $G$ | shear modulus |
| $b$ | Burger's vector |
| $\rho_i$ | local dislocation density |
| $D_0$ | initial grain size |
| $s$ | cell size |
| $K_c$ | calibration constant |
| $\Omega$ | Recovery Function |
| $\Omega_0$ | calibration parameter |
| $\Omega_{r0}$ | calibration parameter |
| $D_v$ | diffusivity |
| $D_{v0}$ | numerical constant |
| $Q_v$ | activation energy |
| $\Delta f_0$ | calibration parameter |
| q | calibration parameter |
| p | calibration parameter |
| $k_b$ | Boltzmann constant |
| $Z$ | Zener-Hollomon parameter |

## 2. Experimental Procedure

*Waspaloy* disks with outer diameter of 127 mm and thickness of 3 mm have been used as workpiece material. Orthogonal roller-burnishing tests were performed using a MAZAK stiff high-speed CNC turning center. Tests were performed using a self-designed roller-burnishing tool, consisting of a hardened steel roller of 40 mm of diameter fastened to a customized crotch. The tool design was based on the work reported by [9]. Tests have been performed in a random order, in order to get reliable results.

The tool holder was connected to a Kistler 9257 piezoelectric dynamometer, for force detection (burnishing force $F_b$ and tangential force $F_t$). Furthermore, an infrared thermo-camera was used to detect the temperature ($T$). Thus, disks were painted with a black thermal-resistant paint in order to guarantee an homogenous value of emissivity.

The experimental setup and the burnishing tool details are shown in Fig. 1.

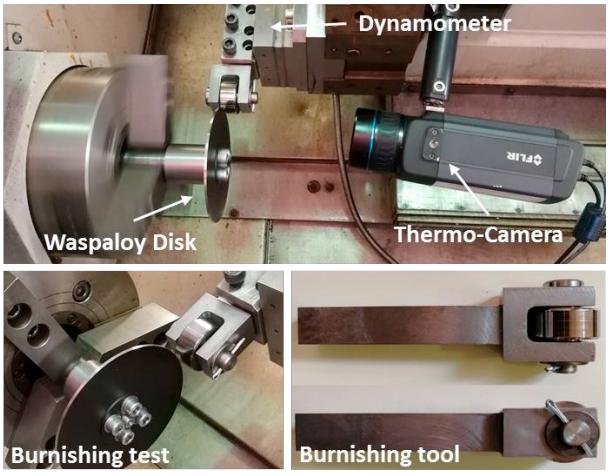


Fig. 1. Experimental setup: disk, dynamometer and thermo-camera position and burnishing tool details.

The experimental tests have been performed at varying burnishing speed ($V_b$), feed rate ($f$) and number of passes ($N$). The lower boundaries of feed rate and speed have been selected according to those available in the literature [6]. The higher values have been further increased from those commonly used, with the aim to have a higher production rate. Also, the number

of passes were chosen within those able to improve both micro-hardness and roughness [10-12]. The complete experimental plan is reported in Table 1.

The effects of burnishing tests have been compared with those of the traditional machining process since they are usually industrially applied as two consecutive steps.

The burnished surfaces obtained of each experimental conditions were cut out from the samples and mounted into a resin holder for microstructural analysis. The samples were mechanically polished and etched using Kalling's reagent N° 2 (5 grams of $CuCl_2$, 100 ml hydrocloridric acid, 100 ml of ethanol). The microstructure was analyzed by means of an optical microscope LEICA DFC 320. Surface roughness were measured using a Mahr surface profilometer. The micro-hardness ($HV_{0.01}$) was measured on polished samples using a QNES10 micro-indenter using 10 s of holding time.

Table 1. Experimental test conditions.

| Burnishing Speed [m/min] | Feed Rate [mm/rev] | Number of Passes |
|---|---|---|
| 40 | 0.05-0.10 | 2-3 |
| 55 | 0.05-0.10 | 2-3 |
| 70 | 0.05-0.10 | 2-3 |
| 100 | 0.05-0.10 | 2-3 |
| 130 | 0.05-0.10 | 2-3 |

## 3. Finite Element Model

A Finite Element model of the roller-burnishing process has been developed using the commercial software SFTC Deform®. A 3D thermo-mechanical multiphysics analysis was performed via Update-Lagrangian code with remeshing technique. FE 3D modeling was based on the assumptions of a rigid burnishing tool (divided into 60000 elements), while the workpiece was modelled as plastic and divided into 150000 tetrahedral elements. The mesh density was increased on the workpiece surface, with a mean element size of 7 µm. The process has been modeled by setting up a fixed workpiece and a linear roto-translational tool obtaining an equivalent condition of the experimental one [3]. The workpiece-tool interaction has been taken into account by setting the global heat transfer coefficient ($h_{int}$ =$10^3$ kW/(m$^2$K)) at the interface according to [13], while friction was modeled as constant ( $10^{-5}$) using Coulomb model for pure rolling conditions [3] (Figure 2).

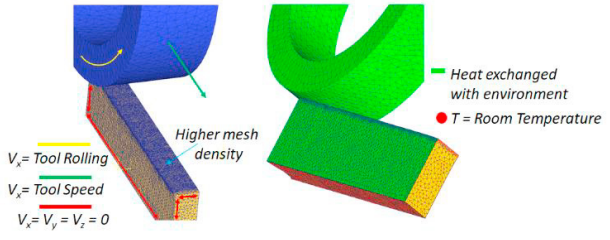


Fig. 2. Movement setup and thermal boundary conditions.

Finally, a physics based constitutive model, presented by the authors in a previous work [8], was employed to describe *Waspaloy* flow stress behavior. The model represents a description of the plastic stress ($\sigma_{pl}$) as algebraic sum of terms describing the contribution to the material plasticity of the different microstructural phenomena occurring during deformation process (Equation 1).

$$\sigma_{pl} = \sigma^* + \sigma_G + \sigma_{HP} \tag{1}$$

Where $\sigma^*$ represents the resistance of the material to plastic deformation where thermal activated mechanisms support the applied stress in moving dislocations through the lattice. $\sigma_{HP}$ is the Hall-Petch stress and indicates the contribution of the grain size to the plastic flow, while $\sigma_G$ designates the strain hardening due to the forest dislocation.

The interaction between the mobile and immobile dislocations is the physical basis of the strengthening of a metal material and is described by well-known Taylor equation (Equation 2).

$$\sigma_G = M\alpha G b\sqrt{\rho_i} \tag{2}$$

Where $\alpha$ is a proportional constant, $M$ is the Taylor factor, $\rho_i$ is the density of immobile dislocations, $G$ is shear modulus and $b$ is the Burger's vector ($2.56^{-10}$ m) [8].

The evolution of the dislocation density is described by the two terms of Equation 3. In detail, $\rho_i^{(+)}$ represents the strengthening effect, while $\rho_i^{(-)}$ represents the softening due to the recovery effects.

$$\dot{\rho}_i = \dot{\rho}_i^{(+)} - \dot{\rho}_i^{(-)} \tag{3}$$

The motion of dislocations can be retarded or stopped by the presence of obstacles causing a hardening effect in the material flow stress. This phenomenon is described by the Equation 4.

$$\dot{\rho}_i^{(+)} = \left(\frac{1}{s} + \frac{1}{D_0}\right)\left(\frac{M}{b}\right)\dot{\bar{\varepsilon}}^p \tag{4}$$

Where $\dot{\bar{\varepsilon}}^p$ is the equivalent plastic strain rate, $D_0$ is the initial grain size and $s$ represents the crystal cell size as described by the Equation 5.

$$s = K_c/\sqrt{\rho_i} \tag{5}$$

$K_c$ is a calibration constant.

The material softening due to recovery effect is reported in Equation 6.

$$\dot{\rho}_i^{(-)} = \Omega\rho_i\dot{\bar{\varepsilon}}^p \tag{6}$$

Where Ω is the recovery function as described by Equation 7 and Equation 8.

$$\Omega = \Omega_0 + \Omega_{r0}\left(\frac{1}{\dot{\bar{\varepsilon}}^p}\frac{D_v}{b^2}\right)^{1/3} \tag{7}$$

$$D_v = D_{v0}exp(-Q_v/k_bT) \tag{8}$$

Where $D_v$ is the diffusivity, while $\Omega_0$ and $\Omega_{r0}$ are two calibration parameters, $D_{v0}$ is a numerical constant, $Q_v$ is the activation energy for self-diffusion. $k_b$ is the Boltzmann constant and $T$ the absolute temperature. The $\sigma^*$ term represents the material resistance to plastic deformation due to the short-range interactions where thermal activated mechanisms assisting the applied stress in moving dislocations and is described by Equation 9.

$$\sigma^* = \sigma_0 \left( 1 - \left( \frac{k_b T}{\Delta f_0 G b^3} ln \left( \frac{\dot{\varepsilon}_{ref}}{\dot{\varepsilon}^p} \right) \right)^{1/q} \right)^{1/p} \quad (9)$$

$\Delta f_0$, $q$ and $p$ are calibration parameter and $\dot{\varepsilon}_{ref}$ is typically taken as $10^6$. The grain size $D$ was predicted taking into account the common mixture law (Equation 10):

$$D = D_{DRX} X_{DRX} + D_0 (1 - X_{DRX}) \quad (10)$$

Where $D_0$ is the average initial grain size (18 μm), $D_{DRX}$ is the dynamically recrystallized grain size (Eq. 11) and $X_{DRX}$ is the volume fraction of the recrystallized grains, this latter is described by the Avrami model (Equation 12).

$$D_{DRX} = 8103 Z^{-0.16} \quad (11)$$

$$X_{DRX} = 1 - exp\left( -log2 \left( \frac{\varepsilon - \varepsilon_{cr}}{\varepsilon_{0.5} - \varepsilon_{cr}} \right)^3 \right) \quad (12)$$

As described in the Equation 12, the $X_{DRX}$ depends on strain $\varepsilon$, critical strain for the nucleation of the recrystallized grains $\varepsilon_{cr}$ (Equation 13), $\varepsilon_{0.5}$ (Equation 14) that is the strain referred to the 50% of recrystallized grains and $Z$ is the Zener-Hollomon parameter described by Equation 15.

$$\varepsilon_{cr} = 0.8 * 5.375 D_0^{0.54} Z^{0.106} \quad (13)$$

$$\varepsilon_{0.5} = 0.1449 D_0^{0.32} Z^{0.14299} \quad (14)$$

$$Z = \dot{\varepsilon}^p exp\left( \frac{468000}{RT} \right) \quad (15)$$

To obtain the correct value of the numerical constants, a fitting procedure of experimental stress-strain curves was carried out.

Table 2. Numerical constants identified.

| Numerical Constant | Value | Numerical Constant | Value |
|---|---|---|---|
| $\alpha$ | 0.35 | $\sigma_0$ [MPa] | 683 |
| $M$ | 3.06 | $\Delta f_0$ | 0.4 |
| $D_{v0}$ [m²/s] | 5.5e-6 | $p$ | 0.27 |
| $Q_v$ [J/mol] | 220000 | $q$ | 1.34 |
| $\Omega_0$ | 10 | $d$ [μm$^{-0.5}$] | 1 |
| $\Omega_{r0}$ | 0.18 | $\upsilon$ | 1.4 |
| $K_c$ | 2.10e+1 | $\alpha_G$ | 2.7 |
| $\rho_0$ [m$^{-2}$] | 5e11 | | |

The value of the constant have been obtained via calibration and by literature analysis as showed in the previous work [8] and are reported in Table 2.

Moreover, the model is able to predict the hardness increasing ($\Delta h$) due to the dislocation accumulation using the numerical model represented by Equation 16.

$$\Delta h = k_h M \alpha G b \sqrt{\rho_i} \quad (16)$$

$k_h$ is a calibration constant and its value is 80.18.

## 4. Results and Discussion

### 4.1. Temperature

Temperatures measured during burnishing tests refer to the maximum value registered during the steady state at the tool-disk interface, referred as "Area of Interest". Fig. 3 (a) and (b) show respectively the temperatures measured during experimental tests and those simulated by the FE model. Fig. 3 (c) reports the thermal fields in both numerical simulation and experimental tests. The temperatures generated during the experimental tests are slightly different from the environment temperature. Nevertheless, although the temperature growth, it is generally recorded that at the more severe working conditions the level of the temperature raise is too low to cause any recrystallization effect. Furthermore, the numerical simulation accurately describes the thermal phenomena taking place during the manufacturing process, showing a maximum error of about 4°C.

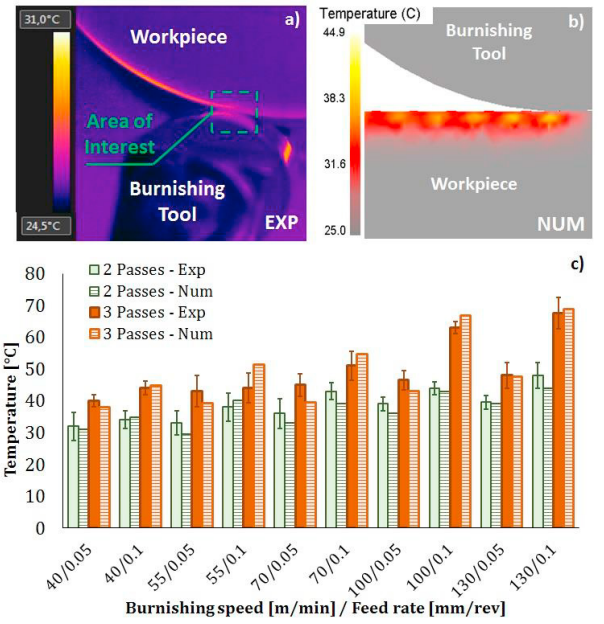


Fig. 3. Experimental measured a) and numerical predicted b) thermal fields and maximum steady state temperatures c) in the area of interest.

### 4.2. Forces

Fig. 4 shows the influence of the process parameters (speed, feed rate and number of passes) on burnishing ($F_b$) and tangential ($F_t$) forces.

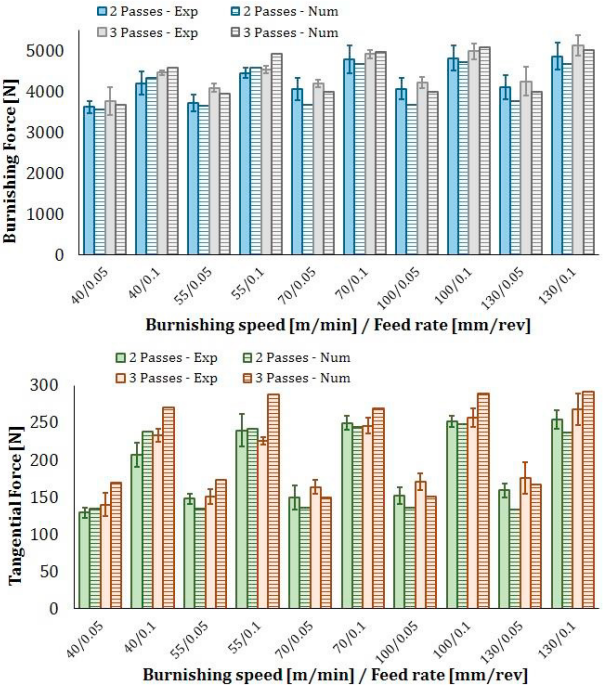


Fig. 4. Experimental measured and numerical simulated steady state burnishing and tangential forces.

It is worth noting that, when the burnishing speed changes from 40 to 130 m/min an evident increase of forces is registered; in particular until 16% for $F_b$ and 26% for $F_t$ at fixed feed rate and number of passes. This effect is due to the strain hardening induced by the higher speed. Thus, considering negligible the temperature increment registered during the experimental tests, no thermal softening effects are detectable while they were significant during machining the same material [6].

Both tangential and burnishing forces slightly increase by increasing of the number of passes, due to the surface hardening at previous passes. Besides, at the increasing of feed rate a significant increment in both forces is noticed due to the deeper deformed layer of workpiece material, with a maximum increment ranging from 11% to 21% for $F_b$ and from 50% to 67% for $F_t$. Comparing the predicted and experimental forces, a global absolute mean error of about 5% is registered for $F_b$ and of nearly 11% for $F_t$, highlighting the good prediction capabilities of the proposed numerical model.

### 4.3. Surface roughness

Achieving a good surface quality with reduced roughness represents a challenge in manufacturing processing such as machining while roller-burnishing represents a useful alternative to common superfinishing processes. Thus, it is relevant to understand a proper combination of burnishing parameters able to effectively improve the surface roughness. In a previous work [6], *Waspaloy* disks were machined with cutting parameters comparable with those used in the present work. In dry machining conditions, the surface roughness is heavily affected from the unavoidable tool wear while it has been verified to be very low in roller-burnishing process. In [6] the average mean surface roughness measured was 2.17 μm, with the lowest value of 1.53 μm reached at highest cutting speed and feed rate (70 m/min and 0.1 mm/rev). Fig. 5 reports the roughness values measured on the samples after burnishing process.

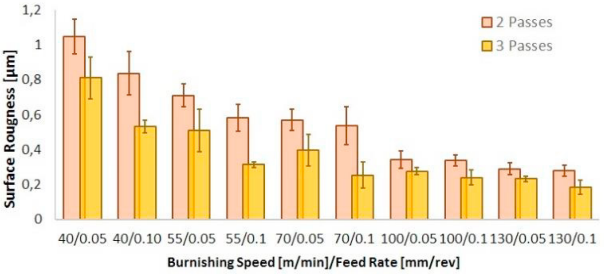


Fig. 5. Surface roughness values on varying burnishing parameters.

Roller-burnishing allows to reach a relevant roughness improvement compared to machining. In all the investigated tests the surface roughness values were always lower than those obtained by machining at comparable parameters. Furthermore, burnishing process is able to reach higher levels of speed and feed rate which are not feasible by machining due to the high wear rate taking place during turning *Waspaloy*. In fact, as also reported by Cobanoglu et al. [14], the surface improvement in terms of roughness is mainly due to the burnishing force which corresponds to high compressive loads compacting the surface [10].

Consequently, when the feed rate and number of passes increase together with the speed, the roughness drastically decreases up to a level where the improvement become less visible.

### 4.4. Microstructure modifications and hardness

Surfaces and sub-surfaces are usually the areas where metallurgical modifications occur during severe plastic deformation processes. In these regions different microscopic phenomena could take place (dislocation accumulation, grain shape modification, dynamic recrystallization, etc.).

The occurrence and entity of these phenomena depend on different combination of strains, strain rates, temperatures and material behavior. In detail, as reported in [8], when *Waspaloy* is subject to aggressive cutting conditions, the coexistence of significant thermal loads, high strain rate and a broad strain field causes significant microstructural changes, such as dynamic recrystallization and intense slip band generation (Fig. 6). On the contrary, the restrained thermal load taking place in roller-burnishing process is not severe enough to induce any

*DRX* phenomena. Thus, the only detectable microstructural modification is an intense grain deformation of the worked surface, especially when heavier process parameters are employed (Fig. 7 a and 7 b).

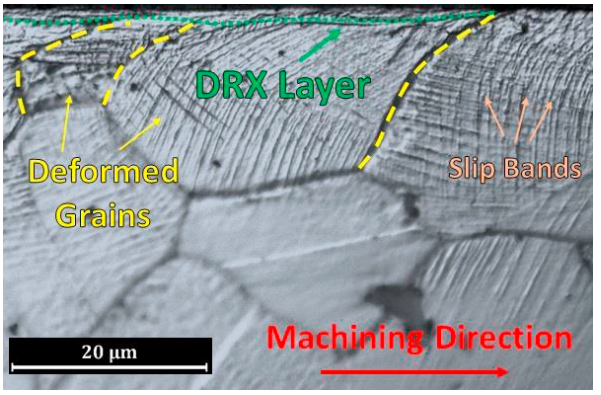


Fig. 6. Microstructural modification in surface and sub-surface under high speed machining (V= 70 m/min, f=0.1 mm/rev, dry conditions) [8].

In both machining and roller burnishing processes the strain fields are consistent; in particular comparing Figs. 7 (a) and (b) it is possible to notice that a higher burnishing speed generates a more intense grain deformation level and a broader affected layer.

Furthermore, comparing machining and roller-burnishing with the same process parameters (speed and feed rate), machining shows a larger affected layer, due to the different thermo-mechanical loads configuration.

Fig. 7 also shows the deformed layer and the numerical predicted strains on the worked surface and sub-surface. The numerical results show wider discrepancies tending to overestimate the dimension of the affected layer. This discrepancy in the prediction of the affected layer thickness, as demonstrated in [15], are strongly related to the mesh size, consequently a higher refining of the mesh on the worked surface is recommended to improve the precision of the solution.

On the other hand, if higher precision is wanted, the needed mesh improvement lead to a consistent increase of the computational time. Thus, a trade off needs to be found.

The strengthening phenomena induced by the plastic deformations of the workpiece surface positively modify the surface and sub-surface hardness. In particular, the work hardening phenomenon is attributed to the role of cross-slip on mobile dislocation generation, rather than slip band formation, consequently the dislocation accumulation is representative of the surface hardening status due to the manufacturing process [16].

Considering that the numerical model takes into account the metallurgical modifications occurring on the deformed material, it represents an important instrument to estimate the dislocations evolution on the workpiece during the manufacturing process.

In particular, a substantial accumulation of dislocations is detected on the surface in terms of dislocation density, as reported in Fig. 8.

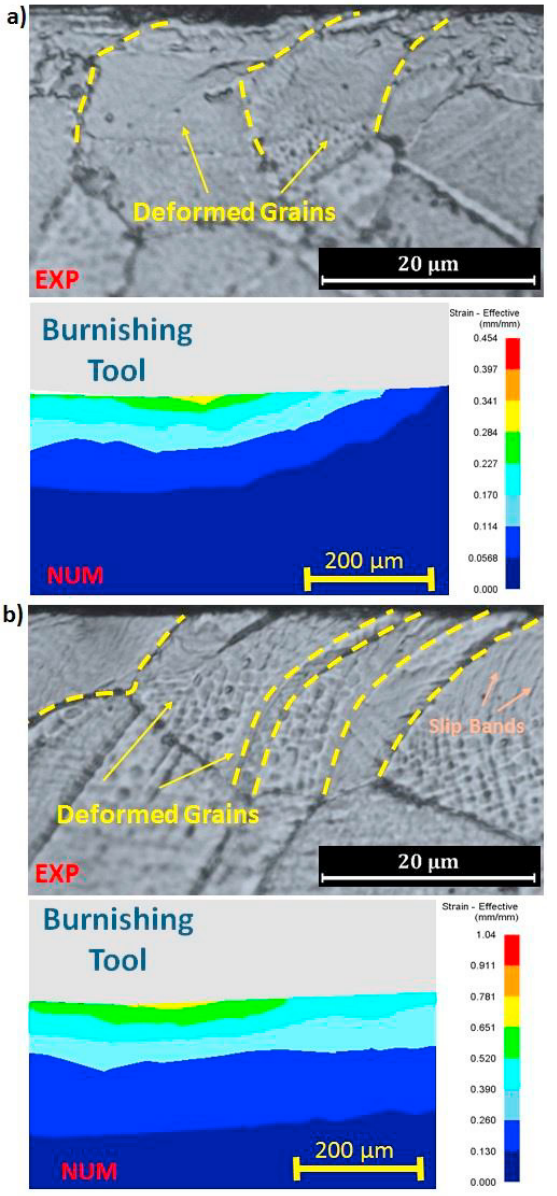


Fig. 7. Microstructural modification in surface and sub-surface under roller-burnishing at a) V= 70 m/min, f=0.1 mm/rev, 3 Passes and b) V= 130 m/min, f=0.1 mm/rev, 3 Passes.

The capability of the numerical model to predict the hardening effect on the worked surface due to dislocation accumulation represents an important instrument to predict the hardness variation providing important feedback for process parameters optimization.

Comparing the results with a previous work on machining [8], it is possible to notice that both machining and roller-burnishing show only little difference on the sub-surface hardness when using similar processing parameters. In contrast, considering that tool wear has a negligible effect in burnishing, heavier processing parameters than dry machining can be used leading to an hardness increment up to a 5% (nearly 20 HV) than that registered by machining.

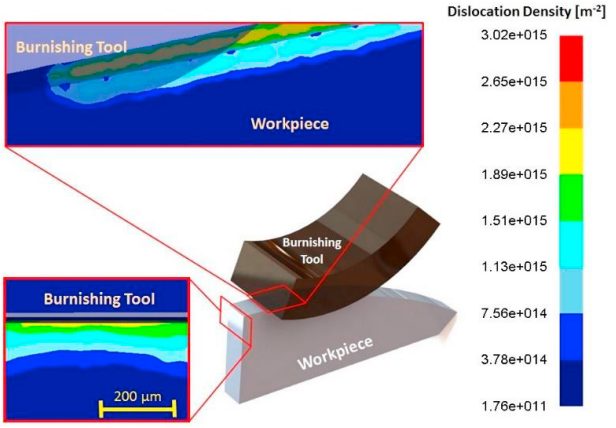


Fig. 8. Dislocation density increment on the burnished surface.

Fig. 9 shows the comparison between the measured and predicted hardness on the worked sub-surface layer; in particular, the hardness value ($HV_{0.01}$) was measured at 10 µm beneath the worked surface. The hardening effect on the surface increases with the increasing of both burnishing speed and feed rate, while the number of passes have a small effect on the hardness variation.

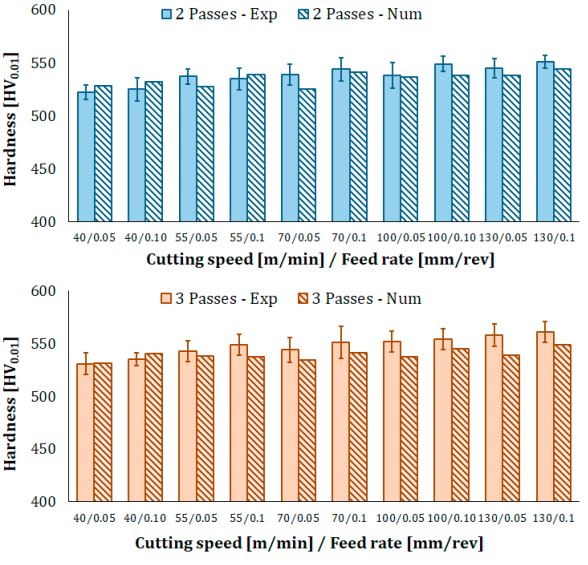


Fig. 9. Hardness values on the burnished sub-surface experimental and numerical predicted on varying burnishing parameters.

The comparison between experimental and numerical predicted hardness is depicted in Fig. 11. Also herein, the numerical prediction in the on the machined near surface is in good agreement with the experimental results, while the prediction error visibly increases through the depth. Thus, the numerical model predicts a deeper hardened layer, as seen for the strain affected layer. The reason lies in the mesh size which should be drastically reduced as also previously pointed out. As overall, the numerical model well predicts the decreasing trend registered in the experimental measurements.

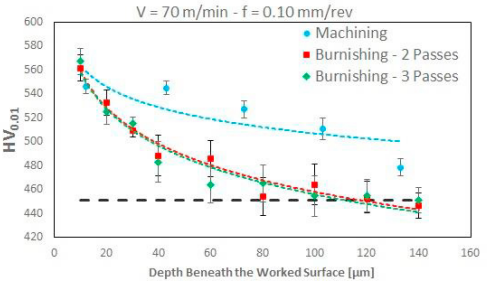


Fig. 10. Hardness profiles at different depth beneath the worked surface, machining and burnishing comparison [8].

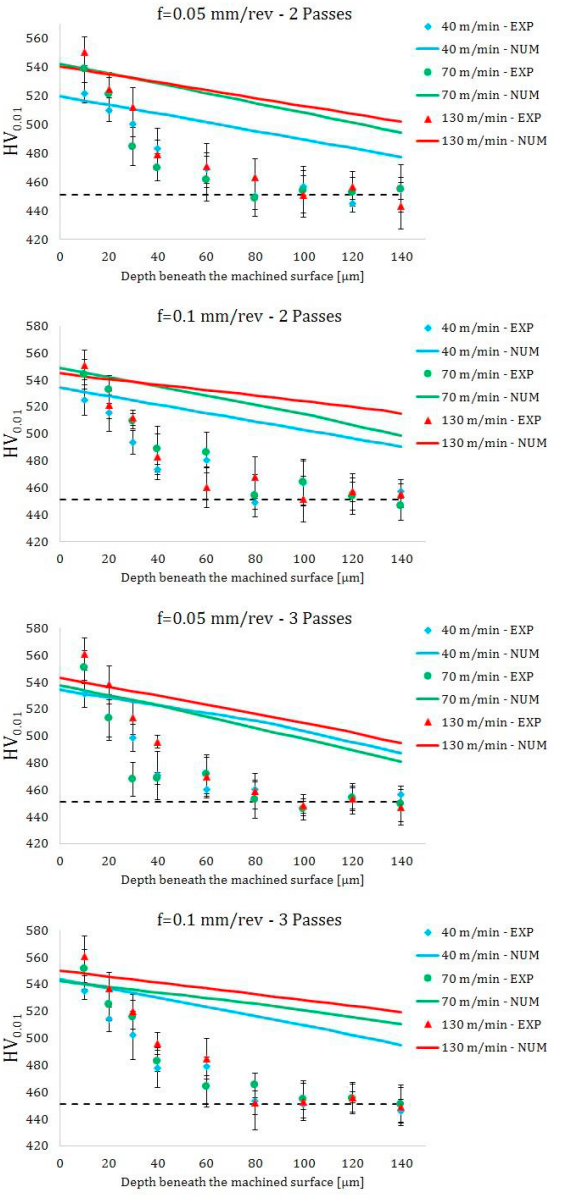


Fig. 11. Comparison between experimental and numerical predicted hardness profiles at different depth beneath the worked surface on varying process parameters.

## 4. Conclusions

In this study a deep analysis of a roller burnishing process on *Waspaloy* is presented. The main process variables have been exploited and the main microstructural modifications have been examined by both experiments and numerical model. The process variables have been analyzed giving important feedback on how to integrate the process into an industrial context. The results also highlight that the final surface roughness is improved at heavier process conditions while grains are clearly deformed as much as the process parameters become more severe. Also, hardness values comparable to machining were noticed, while roller burnishing shows a thinner hardened layer than machining with a better sub surface condition. The numerical prediction of the involved variables is in good agreement with the experimental data, ensuring a useful tool as a support for process parameters optimization.

## References

[1] J. Castro, M. Meggiolaro. Fatigue Design Techniques. CreateSpace 2016, Scotts Valley, CA, USA.

[2] X. Liang, Z. Liu, B. Wang. State-of-the-art of surface integrity induced by tool wear effects in machining process of titanium and nickel alloys: A review. Measurements 132; 2019. p. 150-181.

[3] Y. C. Yen, P. Sartkulvanich, T. Altan. Finite element modeling of roller burnishing process. CIRP Annals 54; 2005. p. 237-240.

[4] G. D. Devaraya Revankar, R. Shetty, S. S. Rao, V. N. Gaitonde. Wear resistance enhancement of titanium alloy (Ti–6Al–4V) by ball burnishing process. J. Mater. Res. Techn. 6; 2017 p. 13-32.

[5] P. Sartkulvanich, T. Altan, F. Jasso, C. Rodriguez. Finite Element Modeling of Hard Roller Burnishing: An Analysis on the Effects of Process Parameters Upon Surface Finish and Residual Stresses. J. Manuf. Sci. Eng 129(4); 2007. p. 705-716

[6] S. Rinaldi, S. Caruso D. Umbrello, L. Filice, R. Franchi, A. Del Prete. Machinability of Waspaloy under different cutting and lubri-cooling conditions. The International Journal of Advanced Manufacturing Technology 94. 2018. p. 9-12.

[7] C. E. Campbell, L. A. Bendersky, W. J. Boettinger, R. Ivester. Microstructural characterization of Al-7075-T651 chips and work pieces produced by high-speed machining. Materials Science and Engineering A 430. 2006. p. 15–26.

[8] S. Imbrogno, S. Rinaldi, D. Umbrello, L. Filice, R. Franchi, A. Del Prete. A physically based constitutive model for predicting the surface integrity in machining of Waspaloy. Materials & Design 152. 2018. p. 140-155.

[9] J. N. Malleswara Rao, C. R. Alavala, M. Sumalatha. Experimental Investigation of the influence of Roller Burnishing Tool Passes on Surface Roughness and Hardness of Brass Specimens. Indian Journal of Science and Technology 04. 2014. p. 142-145.

[10] A. M. Hassan A. S. Al-Bsharat. Influence of burnishing process on surface roughness, hardness, and microstructure of some non-ferrous metals. Wear 199. 1996. p. 1-8.

[11] M.H. El-Axir. An investigation into roller burnishing. International Journal of Machine Tools & Manufacture 40. 2000. p. 1603–1617.

[12] J. Caudill, J. Schoop. I.S. Jawahir. Correlation of surface integrity with processing parameters and advanced interface cooling/lubrication in burnishing of Ti-6Al-4V alloy. Advances in Materials and Processing Technologies 2018.

[13] Z. Pu, D. Umbrello, O. W. Dillon, I. S. Jawahir. Finite Element Simulation of Residual Stresses in Cryogenic Machining of AZ31B Mg Alloy. Procedia CIRP 13. 2014. p. 282 – 287.

[14] T. Cobanoglu, S. Ozturk. Effect of burnishing parameters on the surface quality and hardness. J Engineering Manufacture 229. 2016. p. 1-9.

[15] D. Umbrello, A. Bordin, S. Imbrogno, S. Bruschi. 3D finite element modelling of surface modification in dry andcryogenic machining of EBM Ti6Al4V alloy. CIRP Journal of Manufacturing Science and Technology 18. 2017. p. 92-100.

[16] Z.Q. Wang, I. J. Beyerleina, R. LeSar. Slip band formation and mobile dislocation density generation in high rate deformation of single fcc crystals. Philosophical Magazine 88. 2008. p. 1321-1343.